followed by the association of these complexes with lipid rafts, which triggers dynamin-independent macropinocytosis. After internalization, the endosome pH falls and Tat apparently destabilizes the membranes, which results in a small amount of the endosome contents escaping into the cytosol. The released fraction of Tat can then exert its biologic activity. Consistent with this model, Tat delivery is enhanced by the influenza virus haemagglutinin fusogenic motif, which further destabilizes endosomal membranes at a low pH (Han *et al.*, 2001; Skehel *et al.*, 2001). In cells cotreated with Tat-conjugated HA2 (HA2-Tat), a greater proportion of endocytosed Tat-fused Cre recombinase escapes into the cytoplasm (Wadia *et al.*, 2004). Other studies suggest that certain cell types might incorporate Tat constructs by clathrin- or caveolin-dependent endocytosis, raising the possibility that transport varies according to the cargo or cell type (Ferrari *et al.*, 2003; Fittipaldi *et al.*, 2003; Richard *et al.*, 2005). In addition to the basic Tat peptide, there are other proteins (fragments), such as antennapedia (Antp), Rev and VP22, that enhance cellular uptake of proteins (Table 1) (Derossi *et al.*, 1994; Elliott and O'Hare, 1997; Futaki *et al.*, 2001; Joliot and Prochiantz, 2004). These four well-known PTDs facilitate the delivery of various biomacromolecules into the cell, but few studies have examined their relative efficacy.

In the present study, we evaluated the potency and internalizing pathway of four major PTDs to optimize protein transduction technology and to clarify the mechanisms of action. We also evaluated the cytotoxicity of these four PTDs as this is crucial to their utility as effective biomacromolecule carriers. These analyses may help not only to elucidate the mechanism by which the four peptides facilitate the cellular uptake of biomacromolecules, but also provide criteria for their proper use.

Materials and methods

Cell lines

HeLa cells (human cervical carcinoma cells) and A431 cells (human epithelial carcinoma cells) were obtained from the American Type Culture Collection (Manassas, VA, USA). HaCaT cells (human keratinocyte cells) were kindly provided by Dr S Inui, Osaka University. Jurkat cells (human leukaemia cells) and MOLT-4 cells (human leukaemia cells) were kindly provided by Hayashibara Biochemical Laboratories Inc. (Okayama, Japan). HL60 cells (human promyelocytic leukaemia cells) were obtained from the Japanese Collection of Research Bioresources (JCRB; Osaka, Japan). HeLa cells were cultured in minimal essential medium (MEMα; Wako Pure Chemicals, Osaka, Japan) medium supplemented with 10% fetal bovine serum (FBS) and antibiotics. A431 cells and HaCaT cells were maintained in Dulbecco's modified Eagle's medium (Wako Pure Chemicals) supplemented with 10% FBS, 1% L-glutamine and antibiotics. Jurkat cells and MOLT-4 cells were maintained in RPMI-1640 medium (Wako Pure Chemicals) supplemented with 10% FBS and antibiotics. HL60 cells were maintained in RPMI-1640 medium (Wako Pure Chemicals) supplemented with 20% FBS and antibiotics. All cells were cultured at 37 °C in 5% CO_2.

Table 1 Protein sequences of the PTDs evaluated

PTD	*Origin*	*Sequence*	*pI*
Tat	HIV-1	G**RKKRRQRRR**PPQ	12.70
Antp	*Drosophila*	**RQIKIWFQNRRMKWKK**	12.31
Rev	HIV-1	**TRQARRNRRRRWRERQR**	12.60
VP22	HSV	**NAKTRRHERRRKLAIER**	12.01

The basic amino acids in each sequence are shown in bold.

Synthetic peptides

All peptides used in this study were purchased from the Toray Research Center Inc. (Tokyo, Japan) and had purities above 90%, which was confirmed by high-performance liquid chromatography analysis and mass spectroscopy. The sequences of these peptides were GRKKRRQRRRPPQK-FAM (FAM = carboxyfluorescein) for Tat-conjugated FAM (Tat-FAM), RQIKIWFQNRRMKWKK-FAM for Antp-conjugated FAM (Antp-FAM), TRQARRNRRRRWRERQRK-FAM for Rev-conjugated FAM (Rev-FAM), NAKTRRHERRRKLAIERK-FAM for VP22-conjugated FAM (VP22-FAM), YGRKKRRQRRRK-biotin for Tat-conjugated biotin, RQIKIWFQNRRMKWKKK-biotin Antp-conjugated biotin, TQRARRNRRRRWRERQRK-biotin for Rev-conjugated biotin, NAKTRRHERRRKLAIERK-biotin for VP22-conjugated biotin and GLFEAIEGFIENGWEGMIDGWY GYGRKKRRQRRR for HA2-conjugated Tat (HA2-Tat). The individual PTD sequences are underlined.

Flow cytometric analysis

HeLa cells, HaCaT cells and A431 cells were cultured in 24-well plates (Nalge Nunc International, Naperville, IL, USA) at 5.0×10^4 cells per well in culture medium and incubated for 24 h at 37 °C. Jurkat cells, MOLT-4 cells and HL60 cells were cultured in 24-well plates (Nalge Nunc International) at 1.0×10^5 cells per well in Opti-MEM I (Invitrogen, Carlsbad, CA, USA). After aspirating the media, FAM-conjugated PTD (PTD-FAM) (10 μM) was added to the cells in Opti-MEM I and the culture dishes were incubated for an additional 3 h. Following incubation, the cells were washed with phosphate-buffered saline and incubated for 5 min with 0.1% trypsin to detach them and to remove surface-bound peptides. After incubation, 2 vol of 10% FBS-containing culture medium was added to stop the trypsin activity and to detach the cells completely. The cell suspension was centrifuged at 800 *g*, washed with phosphate-buffered saline, centrifuged again and resuspended in 500 μl of 0.4% paraformaldehyde. Fluorescence was analysed on a FACSCalibur flow cytometer, and data were analysed using CellQuest software (both from Becton Dickinson, San Jose, CA, USA). In the low-temperature uptake experiment, cells were preincubated at 4 °C for 1 h in Opti-MEM I prior to adding the PTDs, and all buffers and solutions were equilibrated to 4 °C. To analyse the internalization mechanism, HeLa cells were pretreated for 30 min in Opti-MEM I medium with 0–5 mM methyl-β-cyclodextrin, 0–2.5 μM

cytochalasin D or 0–5 mM amiloride (all from Sigma-Aldrich, St Louis, MO, USA). After the PTD-FAMs were added, cells were maintained for 1 h (30 min for amiloride) in the presence of inhibitors and washed several times with phosphate-buffered saline. As a control, the cellular uptake of transferrin fluorescein isothiocyanate (Invitrogen) was also monitored.

Cell proliferation assay

Cell viability was determined using a WST-8 assay kit (Nacalai Tesque, Kyoto, Japan) according to the manufacturer's instructions. The assay is based on the cleavage of the tetrazolium salt WST-8 to formazan by cellular mitochondrial dehydrogenase. HeLa cells were cultured in 96-well plates (Nalge Nunc International) at 5.0×10^3 cells per well in MEMα and incubated for 24 h at 37 °C. Jurkat cells were cultured in 96-well plates at 1.0×10^4 cells per well in Dulbecco's modified Eagle's medium. The cells were treated with various concentrations of PTD-biotin. After 24 h incubation, cell viability was measured using the WST-8 assay kit.

Membrane integrity assay

The lactate dehydrogenase (LDH) leakage assay was used to quantify the membrane integrity of the PTD-treated cells. This assay detects the amount of LDH released into the culture media as a result of plasma membrane disruption after PTD treatment. HeLa cells were cultured in 96-well plates (Nalge Nunc International) at 5.0×10^3 cells per well in MEMα and incubated for 24 h at 37 °C. Jurkat cells were cultured in 96-well plates at 1.0×10^4 cells per well in Dulbecco's modified Eagle's medium. Each cell type was treated with various concentrations of PTD-biotin. After 3 h incubation, the LDH release activity of the peptides was measured using an LDH cytotoxicity test (Wako) according to the manufacturer's instructions.

Expression and purification of PTD-fused Venus protein

The Venus (variant of yellow fluorescent protein) DNA sequence was kindly provided by Dr A Miyawaki (RIKEN Brain Science Institute). The Tat-Venus DNA sequence was amplified by PCR. At the 5′ end, the primer sequence 5′-TTTAAGAAGGAGATATACATATGGCTTACGGTCGTAAAAAA CGTCGCCAGCGTCGCCGTGGTGGCGGCGGTTCCCTCGA GCACCACCATCACCACCATGTGAGCAAGGGCGAGGAGC TGTTCAC-3′ introduced an *Nde* I site and Tat sequence and at the 3′ end, the primer sequence 5′-GCTTTGTTAGCAG CCGAATTCTTACTTGTACAGCTCGTCCATGCCGAGAGTGA TC-3′ introduced an *Eco* RI site. The PCR product was digested with *Nde* I and *Eco* RI and inserted into a protein expression plasmid. Other plasmids expressing Antp-, Rev- or VP22-Venus recombinant proteins were constructed by replacing the Tat-coding region in the Tat-Venus plasmid with the Antp, Rev or VP22 sequences using the *Nde* I and *Xho* I restriction sites. These sequences were obtained by annealing the following oligonucleotides with protruding single-strand DNA corresponding to the *Nde* I and *Xho* I sites: Antp sense, 5′-TATGGCTCGTCAGATCAAAATCTGGTTCCA GAATCGTCGTATGAAGTGGAAAAAAGGTGGCGGCGGTTC CC-3′; Antp antisense, 5′-TCGAGGGAACCGCCGCCACCTT TTTTCCACTTCATACGACGATTCTGGAACCAGATTTTGATC TGACGAGCCA-3′; Rev sense, 5′-TATGGCTACCCGTCAGGC TCGTCGTAATCGTCGTCGTCGTTGGCGTGAACGTCAGCGT GGTGGCGGCGGTTCCC-3′; Rev antisense, 5′-TCGAGGGAA CCGCCGCCACCACGCTGACGTTCACGCCAACGACGACGA CGATTACGACGAGCCTGACGGGTAGCCA-3′; VP22 sense, 5′-TATGGCTAACGCTAAAACCCGTCGTCACGAACGTCGTCG TAAACTGGCTATCGAACGTGGTGGCGGCGGTTCCC-3′; VP22 antisense, 5′-TCGAGGGAACCGCCGCCACCACGTTCGATAG CCAGTTTACGACGACGTTCGTGACGACGGGTTTTAGCGT TAGCCA-3′. The plasmids, except for the Antp-Venus expression vector, were transformed into *Escherichia coli* BL21 Star (DE3) (Invitrogen). The Antp-Venus-expressing vector was transformed into BL21 Star (DE3), in which the plasmid-expressing chaperone (pGro7) was pretransformed. Transformed *E. coli* was cultured and the cell paste was suspended in BugBuster Master Mix (Novagen, Darmstadt, Germany) and centrifuged. PTD-Venus was recovered in the supernatant and purified by His-tag affinity purification and gel filtration chromatography.

Confocal laser scanning microscopy analysis

HeLa cells were cultured on Lab-Tek II Chambered Coverglass (Nalge Nunc International) at 3.0×10^4 cells per well in MEMα supplemented with 10% FBS and incubated for 24 h at 37 °C. Internalization of PTD-FAM or PTD-Venus was performed as follows: HeLa cells were treated with PTD-FAM or PTD-Venus (10 μM) in Opti-MEM I containing 100 ng ml^{-1} Hoechst 33342 (Invitrogen) and 6 μg ml^{-1} FM4-64 (Invitrogen). After incubation at 37 °C for 3 h, the medium was exchanged with fresh medium and fluorescence was observed by confocal laser scanning microscopy (Leica Microsystems GmbH, Wetzlar, Germany) without cell fixation. For cotreatment with HA2-Tat, HeLa cells were cotreated with PTD-FAM (10 μM) and HA2-Tat (2 μM) in Opti MEM I containing 100 ng ml^{-1} Hoechst 33342. After incubation at 37 °C for 3 h, the medium was exchanged with fresh medium and fluorescence was observed by confocal laser scanning microscopy without cell fixation.

Results

Comparison of transduction efficiency and cytotoxicity of four PTDs

To confirm the intracellular translocation activity of the four selected PTDs, we evaluated the transduction efficiency of Tat-, Antp-, Rev- and VP22-FAM in six cell lines (adherent: HeLa, HaCaT and A431 cells; nonadherent: Jurkat, MOLT-4 and HL60 cells) using flow cytometric analysis (Figure 1). These PTDs contain a large number of basic amino acids (Table 1) and their cationic properties are thought to be important for cell membrane penetration (Futaki *et al.*, 2001; Chauhan *et al.*, 2007). Their positive charge, however, causes them to adsorb nonspecifically to negatively charged cell

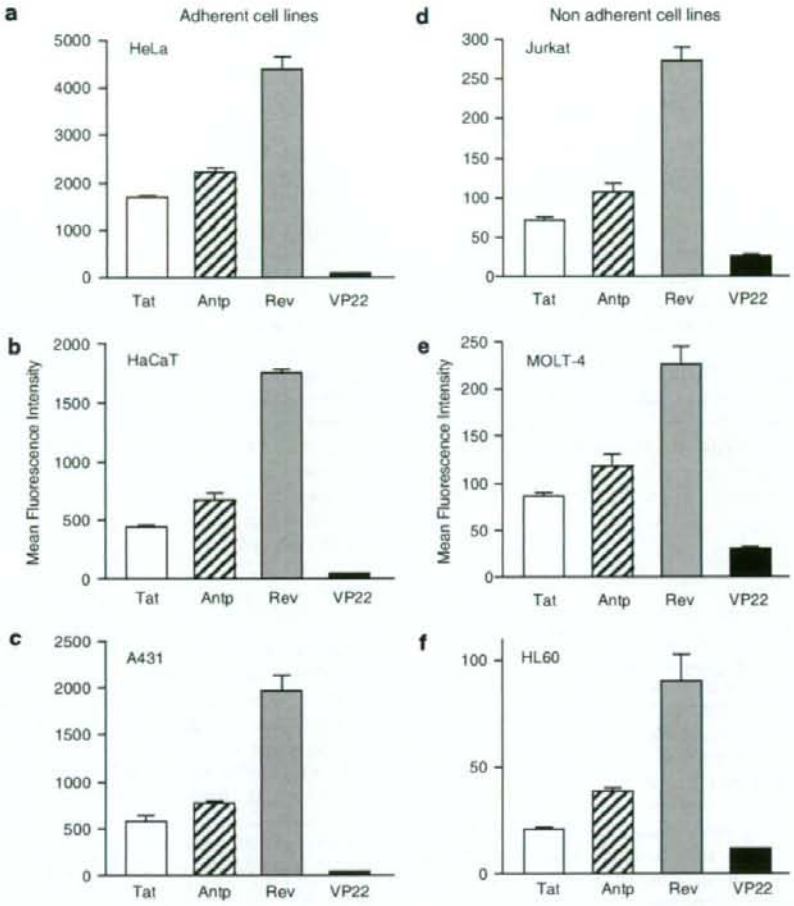

Figure 1 Comparison of the cellular uptake of protein transduction domains (PTDs). FAM-labelled Tat (white column), antennapedia (Antp; hatched column), Rev (grey column) and VP22 (black column) were incubated with six cell lines: HeLa (**a**), HaCaT (**b**), A431 (**c**), Jurkat (**d**), MOLT-4 (**e**) and HL60 (**f**) at 10 μM for 3 h. After trypsin treatment to digest PTDs adsorbed on the cell surface, the PTD-transduced cells were harvested and analysed by flow cytometry. Note that the *y* axis scales for the adherent cell lines are markedly different from that for the nonadherent cell lines. Data shown are the mean ± s.d. of triplicate assays.

membranes (Richard *et al.*, 2003). For this reason, the cells were treated with excess trypsin to eliminate nonspecific plasma membrane binding of the PTDs prior to measurement.

The relative order of their translocation efficiency (Rev > Antp > Tat > VP22), which was based on mean fluorescence, was independent of the cell type (that is, adherent or nonadherent). Furthermore, using PTD-fused Venus, we confirmed that Rev had the highest transduction efficiency (data not shown). Equally important, the overall translocation efficiency of the PTDs depended markedly on whether the cells were adherent (HeLa, HaCaT and A431 cells) or nonadherent (Jurkat, MOLT-4 and HL60 cells). The transduction efficiency was much higher in the adherent cell lines compared with the nonadherent cell lines (Figure 1); note that that the fluorescence (uptake) was about 8- to 25-fold greater in the adherent, than in nonadherent, cell lines.

The cytotoxic properties of the four PTDs were evaluated in adherent (HeLa) and nonadherent (Jurkat) cells. To assess the long-term changes in proliferation, mitochondrial dehydrogenase activity was measured using a WST-8 assay 24 h after PTD treatment. In HeLa cells, there was a remarkable decrease in cell viability when the cells were incubated with Antp at 100 μM, whereas other PTDs were not cytotoxic at the higher concentrations (Figure 2a). In contrast in Jurkat cells, Antp was extremely cytotoxic in a dose-dependent manner and Rev reduced cell proliferation by approximately 40% (Figure 2b). Previous reports indicated that amphipathic peptides, such as transportan, induced cytotoxicity by perturbing the cellular membrane (Hallbrink *et al.*, 2001; Jones *et al.*, 2005; Saar *et al.*, 2005; El-Andaloussi *et al.*, 2007). Thus, the membrane integrity of PTD-treated cells was also measured using an LDH leakage assay. Antp

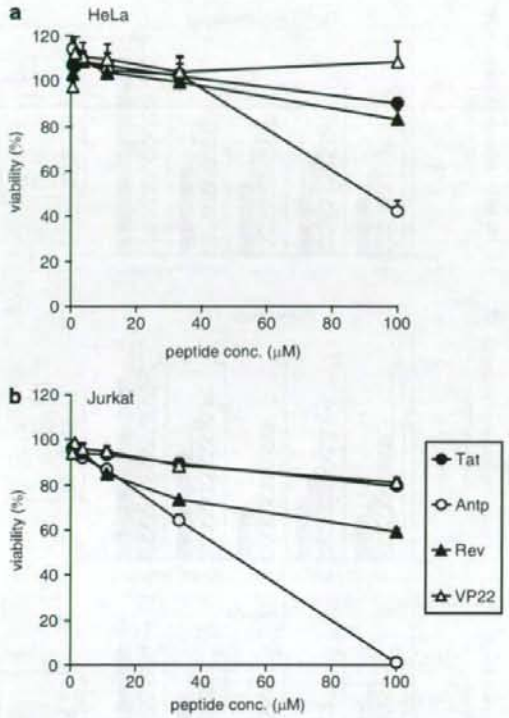

Figure 2 Viability of protein transduction domain (PTD)-treated cells. HeLa cells (**a**) and Jurkat cells (**b**) were incubated with serially diluted biotin-conjugated Tat, antennapedia (Antp), Rev and VP22 at 37 °C. After 24 h, cell viability was analysed using a WST-8 assay. Data shown are the mean ± s.d. of triplicate assays.

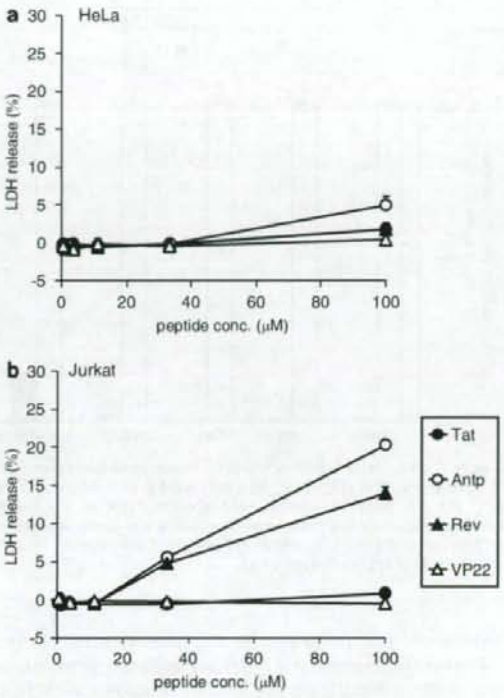

Figure 3 Membrane integrity of protein transduction domain (PTD)-treated cells. HeLa cells (**a**) and Jurkat cells (**b**) were incubated with serially diluted biotin-conjugated Tat, antennapedia (Antp), Rev and VP22 at 37 °C. After 3 h, the release of lactate dehydrogenase (LDH) was analysed. Data shown are the mean ± s.d. of triplicate assays.

and Rev induced significant LDH leakage in Jurkat cells, but only low LDH leakage was detected in Antp-treated HeLa cells (Figure 3). The membrane-perturbing effect of Antp and Rev contributed to the uptake of peptides, which are shown in Figure 1. Jurkat cells appear more sensitive to Antp or Rev treatment than HeLa cells; this difference in cytotoxicity and translocation efficiency may indicate a difference in the PTD-uptake mode.

Intracellular transduction mechanism of PTDs

The results of *in vitro* studies suggest that PTDs enter the cell via an energy-dependent endocytotic pathway (Lundberg *et al.*, 2003; Richard *et al.*, 2003). In particular, studies using various macropinocytosis inhibitors, such as methyl-β-cyclodextrin, to deplete cholesterol from the membrane (Grimmer *et al.*, 2002; Liu *et al.*, 2002), cytochalasin D, to inhibit F-actin elongation (Sampath and Pollard, 1991), or amiloride, to inhibit the Na^+-H^+ exchanger (West *et al.*, 1989), indicate that Tat is taken up into the cell via lipid raft-dependent macropinocytosis. To the best of our knowledge, however, few comparative studies have analysed the cellular uptake pathway of the four PTDs discussed in this paper. Therefore, we used flow cytometry analysis to determine whether PTD uptake is energy dependent or occurs via lipid raft-mediated macropinocytosis. First, we treated cells with PTD-FAM at 37 or 4 °C and then measured cell fluorescence (Figure 4). At 4 °C, transferrin, which enters cells by clathrin-dependent endocytosis (Schmid, 1997), inhibited the transduction efficiency compared with that at 37 °C. All four PTDs had low transduction ability at 4 °C, indicating that their cellular uptake was energy dependent. We next examined the PTD-FAM uptake efficiency in methyl-β-cyclodextrin-, cytochalasin D- and amiloride-treated HeLa cells. These cell treatments inhibited PTD-FAM incorporation in a dose-dependent manner, but transferrin was not affected (Figure 5). Furthermore, in HeLa cells treated with PTD-FAM, only punctuate fluorescence was observed using confocal laser scanning microscopic analysis (Figure 6). These results indicated that all the PTDs evaluated in this study enter the cell through the macropinocytotic pathway and that most of them were trapped in intracellular vesicles, the macropinosomes.

Intracellular localization of PTD–protein conjugates

We next examined the intracellular behaviour of the individual PTDs in more detail. To investigate whether

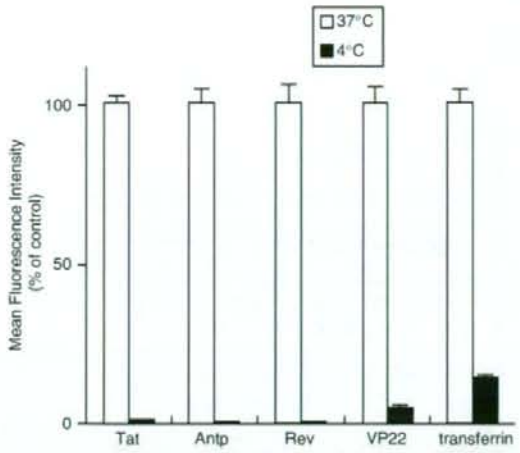

Figure 4 Effects of temperature on protein transduction domain (PTD) transduction efficiency. HeLa cells were preincubated at 37 or 4 °C for 1 h prior to adding FAM-labelled PTDs or fluorescein isothiocyanate-labelled transferrin for 3 h. Cells were washed in trypsin and analysed by flow cytometry. Data shown are the mean ± s.d. of triplicate assays.

individual PTDs are located in the same vesicles, we used Tat-fused HA2 peptide (HA2-Tat), an influenza virus-derived endosome-disrupting peptide. HA2-Tat improves the activity of Tat-fused Cre recombinase (Wadia *et al.*, 2004). Because HA2 alone cannot enter the cell, HA2-Tat is thought to enter the cell in a Tat-dependent manner and to disrupt the membrane of endosomal vesicles in which the Tat cargo is trapped. Thus, if Antp, Rev and VP22 are trapped in the same vesicles as Tat, the fluorescence should spread throughout the cytosol following cotreatment of the cells with HA2-Tat. As predicted, in HeLa cells cotreated with Antp-, Rev- or VP22-Venus and HA2-Tat, the Venus-derived fluorescence spread throughout the cytosol, whereas in the cells treated with Antp-, Rev- or VP22-Venus alone, only punctuate fluorescence was observed (Figure 7). These results suggested that all the PTDs evaluated in this study entered the cell through a macropinocytotic pathway and were trapped in the same vesicles as Tat.

Discussion

In the present study, we have systematically compared PTD-mediated molecular transduction mechanisms. Our findings indicated that individual PTDs have different levels of transduction efficiency and cytotoxicity, suggesting that PTDs are internalized into live cells via different mechanisms. We also examined the internalization pathway and intracellular localization of Tat, Antp, Rev and VP22. Unexpectedly, all the PTDs evaluated in this study entered the cell through the macropinocytotic pathway and were trapped in the same vesicles as Tat. The finding that the intracellular transduction pathways of the four PTDs were the same suggests that the method of cell internalization does not contribute to the

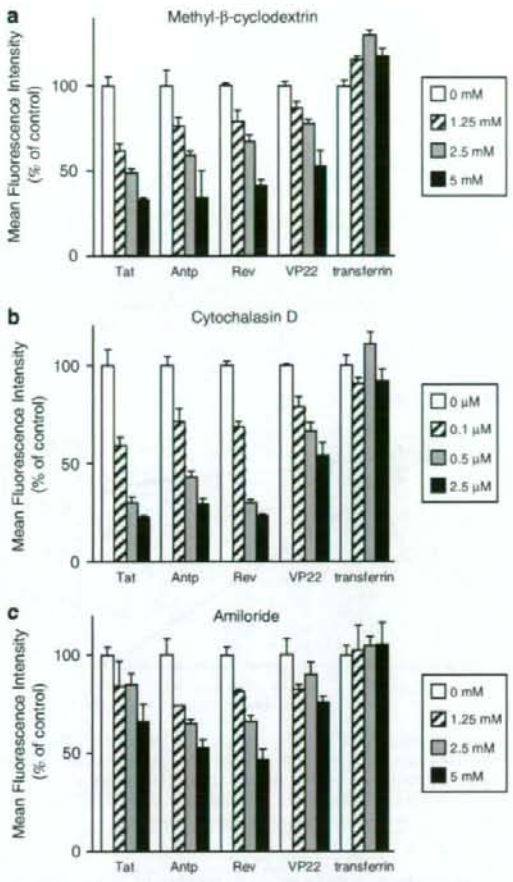

Figure 5 Effects of endocytosis inhibitors on transduction efficiency of protein transduction domains (PTDs). HeLa cells were pretreated with a range of concentrations of (**a**) methyl-β-cyclodextrin, (**b**) cytochalasin D or (**c**) amiloride for 30 min prior to adding FAM-labelled PTDs or fluorescein isothiocyanate-labelled transferrin for 1 h (**a** and **b**) or 30 min (**c**). Cells were washed in trypsin and analysed by flow cytometry. Data shown are the mean ± s.d. of triplicate assays.

differences in the PTD transduction efficiency or cytotoxicity. Although the reason for this phenomenon is not clear, we speculate that the primary structure of the individual PTDs or the cell surface proteins that interact with the individual PTDs contribute to the differences in their transduction efficiency and cytotoxicity.

The initial step in the mechanism of cellular entry of PTDs is thought to be the strong ionic interaction between the amino-acid residues of the PTDs and the plasma membrane constituents. Because the translocation is solely physically mediated, the charge distribution and amphipathicity of the peptide and its interaction with the plasma membrane is critical (Pujals *et al.*, 2006). Although most PTDs, if not all, contain a large number of basic amino acids, such as arginine or lysine, the theoretical isoelectric point (pI) value of each PTD used in this study was essentially identical (Tat, Antp,

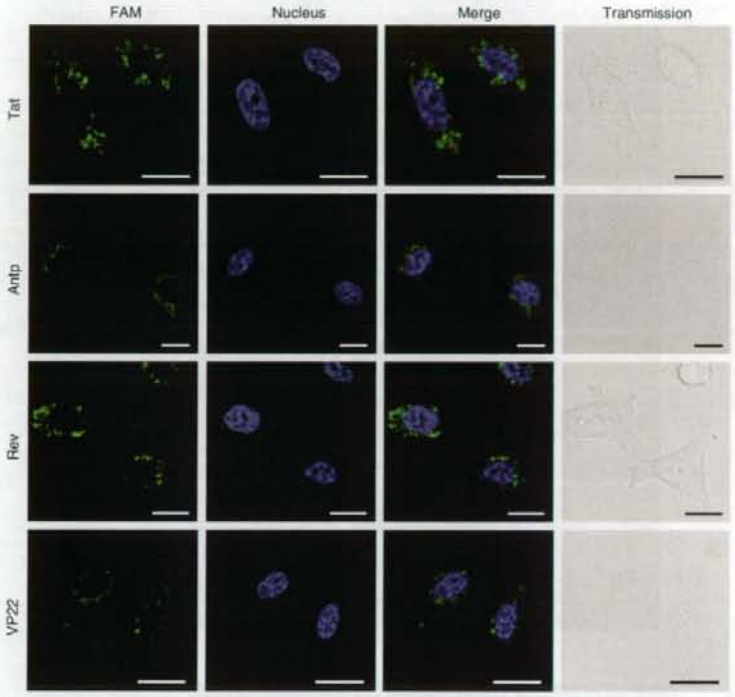

Figure 6 Intracellular behaviour of protein transduction domain (PTD)-FAM in living cells. HeLa cells were treated with 10 μM PTD-FAM for 3 h. Fluorescence images were acquired using confocal laser scanning microscopy and the signals were merged electronically. The nucleus was counterstained with Hoechst 33342 (blue). From top to bottom: Tat-, antennapedia (Antp)-, Rev- and VP22-FAM. From left to right: FAM (green), nucleus (blue), merged fluorescence and transmission image. Scale bars in each microphotograph indicate 20 μm.

Rev and VP22 have pI values of 12.70, 12.31, 12.60 and 12.01, respectively). Therefore, the internalization efficiency does not appear to depend on the cationic features of the PTDs.

The amphipathicity of the carrier is probably responsible not only for the strong interaction with the lipid membranes (Yandek *et al.*, 2007), but also for the disruption of the cellular membrane, which results in cell death (Hallbrink *et al.*, 2001; Jones *et al.*, 2005; Saar *et al.*, 2005; El-Andaloussi *et al.*, 2007). In terms of cytotoxicity, our data indicate that Antp and Rev both disrupt the membrane (Figure 3), but Rev does not contain an amphipathic structure. Furthermore, there was no correlation between hydrophobicity and transduction efficiency. Thus, differences in the PTD-mediated transduction efficiency and cytotoxicity might be due to the molecular weight or pI of the conjugated cargo.

The cellular events required for internalization, however, differ between reports and are often conflicting. The first mechanistic studies led to the proposal that PTD internalization occurs rapidly in a receptor- and energy-independent manner, perhaps by destabilizing the lipid bilayer or by the formation of inverted micelles with subsequent release of their contents within the intracellular space (Berlose *et al.*, 1996). More recently, an active mechanism based on vesicular uptake was proposed as the general mode of cell internalization of PTDs. In our experiment, although all four PTDs tended to be present in the same vesicles, the detailed mechanism for this colocalization is not yet known. It has been suggested that PTD internalization requires cell surface heparan sulphate proteoglycans (Tyagi *et al.*, 2001; Console *et al.*, 2003; Ziegler and Seelig, 2004). Because Tat interacts electrostatically with heparan sulphate proteoglycan present on the cell surface, it is possible that some PTDs are taken into the same vesicles when they interact with one heparan sulphate proteoglycan. In contrast, as shown in Figure 7, although fluorescence was observed throughout the cytosol, punctate fluorescence was also observed when the cells were cotreated with PTD-Venus and HA2-Tat. This finding suggested that the PTDs did not all exist in the same vesicles and that some PTDs entered the cell through another pathway. This is just speculation, however, and we are now using proteome analysis, such as liquid chromatography coupled with mass spectrometry or two-dimensional gel electrophoresis, to examine whether there are individual cell surface receptors for different PTDs.

In summary, our data suggest that Antp, Rev, VP22 and Tat cross the plasma membrane and reach the macropinosomes via different mechanisms. Our findings also indicate that several issues, such as endosome entrapment and low cell specificity, which limit the therapeutic activity of the cargo,

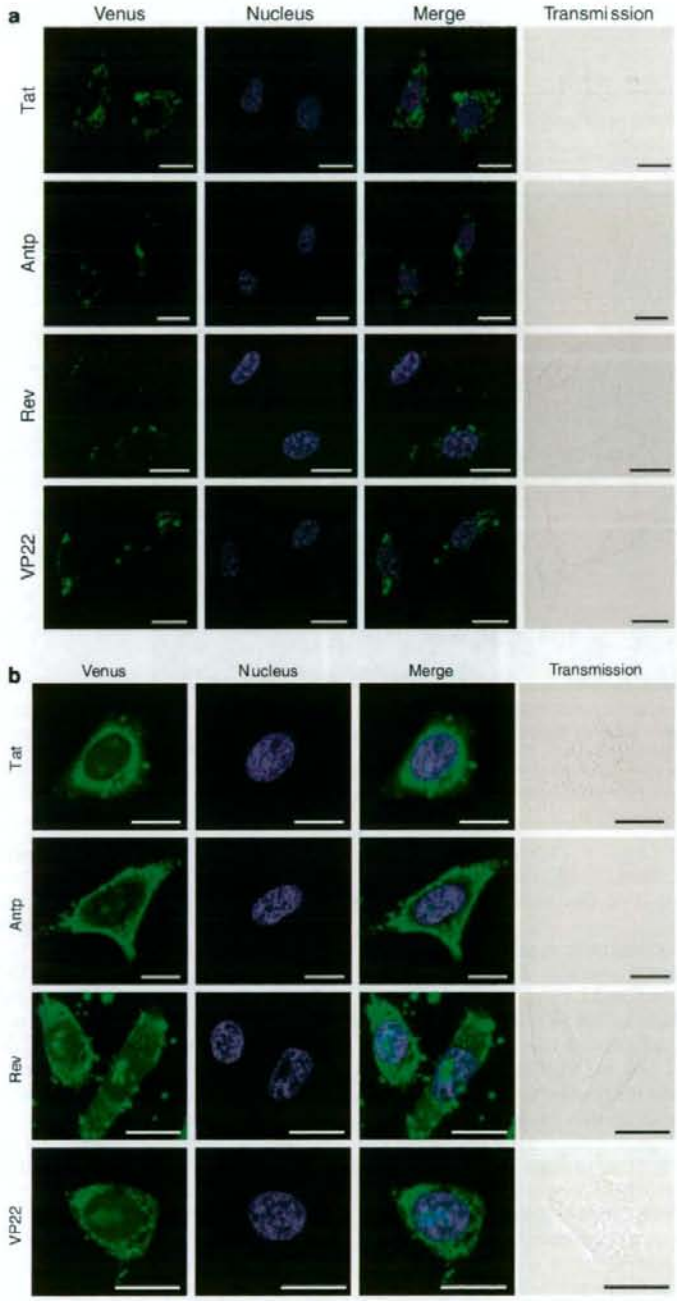

Figure 7 Intracellular behaviour of protein transduction domain (PTD)-Venus in living cells. HeLa cells were treated with 10 μM PTD-Venus alone (**a**) or 10 μM HA2-Tat (**b**) for 3 h. Fluorescence images were acquired using confocal laser scanning microscopy and the signals were merged electronically. The nucleus was counterstained with Hoechst 33342 (blue). From top to bottom: Tat-, antennapedia (Antp)-, Rev- and VP22-Venus. From left to right: Venus (green), nucleus (blue), merged fluorescence and transmission image. Scale bars in each microphotograph indicate 20 μm.

must be overcome before effective PTD-based drug delivery carriers can be fully developed. We previously reported that cotreatment with HA2-Tat enhances the cytosolic release of Tat-fused peptide-blockers and their biological activities, thereby overcoming the issue of endosome entrapment (Sugita *et al.*, 2007). Furthermore, although the transduction mechanism of PTDs is not yet well understood, these differences led us to explore the possibility of creating novel PTDs. We successfully created novel PTDs that have higher transduction efficiencies than Tat, using a unique phage display-based screening strategy that we previously developed (Mukai *et al.*, 2006; Kamada *et al.*, 2007). Moreover, based on our PTD-screening system, we are currently working to create more useful PTDs with cell type specificity.

Conflict of interest

The authors state no conflict of interest.

References

Berlose JP, Convert O, Derossi D, Brunissen A, Chassaing G (1996). Conformational and associative behaviours of the third helix of antennapedia homeodomain in membrane-mimetic environments. *Eur J Biochem* **242**: 372–386.

Borsello T, Forloni G (2007). JNK signalling: a possible target to prevent neurodegeneration. *Curr Pharm Des* **13**: 1875–1886.

Brusic V, Marina O, Wu CJ, Reinherz EL (2007). Proteome informatics for cancer research: from molecules to clinic. *Proteomics* **7**: 976–991.

Chauhan A, Tikoo A, Kapur AK, Singh M (2007). The taming of the cell penetrating domain of the HIV Tat: myths and realities. *J Control Release* **117**: 148–162.

Console S, Marty C, Garcia-Echeverria C, Schwendener R, Ballmer-Hofer K (2003). Antennapedia and HIV transactivator of transcription (TAT) 'protein transduction domains' promote endocytosis of high molecular weight cargo upon binding to cell surface glycosaminoglycans. *J Biol Chem* **278**: 35109–35114.

Derossi D, Joliot AH, Chassaing G, Prochiantz A (1994). The third helix of the Antennapedia homeodomain translocates through biological membranes. *J Biol Chem* **269**: 10444–10450.

Drabik A, Bierczynska-Krzysik A, Bodzon-Kulakowska A, Suder P, Kotlinska J, Silberring J (2007). Proteomics in neurosciences. *Mass Spectrom Rev* **26**: 432–450.

El-Andaloussi S, Jarver P, Johansson HJ, Langel U (2007). Cargo dependent cytotoxicity and delivery efficacy of cell-penetrating peptides: a comparative study. *Biochem J* **407**: 285–292.

Elliott G, O'Hare P (1997). Intercellular trafficking and protein delivery by a herpesvirus structural protein. *Cell* **88**: 223–233.

Ferrari A, Pellegrini V, Arcangeli C, Fittipaldi A, Giacca M, Beltram F (2003). Caveolae-mediated internalization of extracellular HIV-1 tat fusion proteins visualized in real time. *Mol Ther* **8**: 284–294.

Fittipaldi A, Ferrari A, Zoppe M, Arcangeli C, Pellegrini V, Beltram F *et al.* (2003). Cell membrane lipid rafts mediate caveolar endocytosis of HIV-1 Tat fusion proteins. *J Biol Chem* **278**: 34141–34149.

Futaki S, Suzuki T, Ohashi W, Yagami T, Tanaka S, Ueda K *et al.* (2001). Arginine-rich peptides. An abundant source of membrane-permeable peptides having potential as carriers for intracellular protein delivery. *J Biol Chem* **276**: 5836–5840.

Grimmer S, van Deurs B, Sandvig K (2002). Membrane ruffling and macropinocytosis in A431 cells require cholesterol. *J Cell Sci* **115**: 2953–2962.

Hallbrink M, Floren A, Elmquist A, Pooga M, Bartfai T, Langel U (2001). Cargo delivery kinetics of cell-penetrating peptides. *Biochim Biophys Acta* **1515**: 101–109.

Han X, Bushweller JH, Cafiso DS, Tamm LK (2001). Membrane structure and fusion-triggering conformational change of the fusion domain from influenza hemagglutinin. *Nat Struct Biol* **8**: 715–720.

Hawiger J (1999). Noninvasive intracellular delivery of functional peptides and proteins. *Curr Opin Chem Biol* **3**: 89–94.

Joliot A, Prochiantz A (2004). Transduction peptides: from technology to physiology. *Nat Cell Biol* **6**: 189–196.

Jones SW, Christison R, Bundell K, Voyce CJ, Brockbank SM, Newham P *et al.* (2005). Characterisation of cell-penetrating peptide-mediated peptide delivery. *Br J Pharmacol* **145**: 1093–1102.

Kamada H, Okamoto T, Kawamura M, Shibata H, Abe Y, Ohkawa A *et al.* (2007). Creation of novel cell-penetrating peptides for intracellular drug delivery using systematic phage display technology originated from Tat transduction domain. *Biol Pharm Bull* **30**: 218–223.

Kaplan IM, Wadia JS, Dowdy SF (2005). Cationic TAT peptide transduction domain enters cells by macropinocytosis. *J Control Release* **102**: 247–253.

Liu NQ, Lossinsky AS, Popik W, Li X, Gujuluva C, Kriederman B *et al.* (2002). Human immunodeficiency virus type 1 enters brain microvascular endothelia by macropinocytosis dependent on lipid rafts and the mitogen-activated protein kinase signaling pathway. *J Virol* **76**: 6689–6700.

Lundberg M, Wikstrom S, Johansson M (2003). Cell surface adherence and endocytosis of protein transduction domains. *Mol Ther* **8**: 143–150.

Mukai Y, Sugita T, Yamato T, Yamanada N, Shibata H, Imai S *et al.* (2006). Creation of novel protein transduction domain (PTD) mutants by a phage display-based high-throughput screening system. *Biol Pharm Bull* **29**: 1570–1574.

Murriel CL, Dowdy SF (2006). Influence of protein transduction domains on intracellular delivery of macromolecules. *Expert Opin Drug Deliv* **3**: 739–746.

Nagahara H, Vocero-Akbani AM, Snyder EL, Ho A, Latham DG, Lissy NA *et al.* (1998). Transduction of full-length TAT fusion proteins into mammalian cells: TAT-p27Kip1 induces cell migration. *Nat Med* **4**: 1449–1452.

Nori A, Kopecek J (2005). Intracellular targeting of polymer-bound drugs for cancer chemotherapy. *Adv Drug Deliv Rev* **57**: 609–636.

Pujals S, Fernandez-Carneado J, Lopez-Iglesias C, Kogan MJ, Giralt E (2006). Mechanistic aspects of CPP-mediated intracellular drug delivery: relevance of CPP self-assembly. *Biochim Biophys Acta* **1758**: 264–279.

Rhodes DR, Chinnaiyan AM (2005). Integrative analysis of the cancer transcriptome. *Nat Genet* **37** (Suppl): S31–S37.

Richard JP, Melikov K, Brooks H, Prevot P, Lebleu B, Chernomordik LV (2005). Cellular uptake of unconjugated TAT peptide involves clathrin-dependent endocytosis and heparan sulfate receptors. *J Biol Chem* **280**: 15300–15306.

Richard JP, Melikov K, Vives E, Ramos C, Verbeure B, Gait MJ *et al.* (2003). Cell-penetrating peptides. A reevaluation of the mechanism of cellular uptake. *J Biol Chem* **278**: 585–590.

Rojas M, Donahue JP, Tan Z, Lin YZ (1998). Genetic engineering of proteins with cell membrane permeability. *Nat Biotechnol* **16**: 370–375.

Saar K, Lindgren M, Hansen M, Eiriksdottir E, Jiang Y, Rosenthal-Aizman K *et al.* (2005). Cell-penetrating peptides: a comparative membrane toxicity study. *Anal Biochem* **345**: 55–65.

Sampath P, Pollard TD (1991). Effects of cytochalasin, phalloidin, and pH on the elongation of actin filaments. *Biochemistry* **30**: 1973–1980.

Schmid SL (1997). Clathrin-coated vesicle formation and protein sorting: an integrated process. *Annu Rev Biochem* **66**: 511–548.

Schwarze SR, Ho A, Vocero-Akbani A, Dowdy SF (1999). *In vivo* protein transduction: delivery of a biologically active protein into the mouse. *Science* **285**: 1569–1572.

Schwarze SR, Hruska KA, Dowdy SF (2000). Protein transduction: unrestricted delivery into all cells? *Trends Cell Biol* **10**: 290–295.

Skehel JJ, Cross K, Steinhauer D, Wiley DC (2001). Influenza fusion peptides. *Biochem Soc Trans* **29**: 623–626.

Sugita T, Yoshikawa T, Mukai Y, Yamanada N, Imai S, Nagano K *et al.* (2007). Improved cytosolic translocation and tumor-killing

activity of Tat-shepherdin conjugates mediated by co-treatment with Tat-fused endosome-disruptive HA2 peptide. *Biochem Biophys Res Commun* **363**: 1027–1032.

Tyagi M, Rusnati M, Presta M, Giacca M (2001). Internalization of HIV-1 tat requires cell surface heparan sulfate proteoglycans. *J Biol Chem* **276**: 3254–3261.

Wadia JS, Stan RV, Dowdy SF (2004). Transducible TAT-HA fusogenic peptide enhances escape of TAT-fusion proteins after lipid raft macropinocytosis. *Nat Med* **10**: 310–315.

West MA, Bretscher MS, Watts C (1989). Distinct endocytotic pathways in epidermal growth factor-stimulated human carcinoma A431 cells. *J Cell Biol* **109**: 2731–2739.

Yandek LE, Pokorny A, Floren A, Knoelke K, Langel U, Almeida PF (2007). Mechanism of the cell-penetrating peptide transportan 10 permeation of lipid bilayers. *Biophys J* **92**: 2434–2444.

Ziegler A, Seelig J (2004). Interaction of the protein transduction domain of HIV-1 TAT with heparan sulfate: binding mechanism and thermodynamic parameters. *Biophys J* **86**: 254–263.

doi:10.1016/j.jmb.2008.05.047 J. Mol. Biol. (2008) 380, 777–782

JMB

Available online at www.sciencedirect.com

ScienceDirect

ELSEVIER

COMMUNICATION

Organelle-Targeted Delivery of Biological Macromolecules Using the Protein Transduction Domain: Potential Applications for Peptide Aptamer Delivery into the Nucleus

Tomoaki Yoshikawa[1,2]†, Toshiki Sugita[1,2]†, Yohei Mukai[1,2], Natsue Yamanada[1,2], Kazuya Nagano[1,2], Hiromi Nabeshi[1,2], Yasuo Yoshioka[1,3], Shinsaku Nakagawa[2], Yasuhiro Abe[1], Haruhiko Kamada[1,3], Shin-ichi Tsunoda[1,3]* and Yasuo Tsutsumi[1,2,3]

[1]*Laboratory of Pharmaceutical Proteomics, National Institute of Biomedical Innovation, 7-6-8 Saito-Asagi, Ibaraki, Osaka 567-0085, Japan*

[2]*Graduate School of Pharmaceutical Sciences, Osaka University, 1-6 Yamadaoka, Suita, Osaka 565-0871, Japan*

[3]*The Center for Advanced Medical Engineering and Informatics, Osaka University, 1-6 Yamadaoka, Suita, Osaka 565-0871, Japan*

Received 5 March 2008; received in revised form 16 May 2008; accepted 21 May 2008
Available online 29 May 2008

Edited by J. Karn

Extensive effort is currently being expended on the innovative design and engineering of new molecular carrier systems for the organelle-targeted delivery of biological cargoes (e.g., peptide aptamers or biological proteins) as tools in cell biology and for developing novel therapeutic approaches. Although cell-permeable Tat peptides are useful carriers for delivering biological molecules into the cell, much internalized Tat-fused cargo is trapped within macropinosomes and thus not delivered into organelles. Here, we devised a novel intracellular targeting technique to deliver Tat-fused cargo into the nucleus using an endosome-disruptive peptide (hemagglutinin-2 subunit) and a nuclear localization signal peptide. We show for the first time that Tat-conjugated peptide aptamers can be selectively delivered to the nucleus by using combined hemagglutinin-2 subunit and nuclear localization signal peptides. This nuclear targeting technique resulted in marked enhancement of the cytostatic activity of a Tat-fused p53-derived peptide aptamer against human MDM2 (mouse double minute 2) that inhibits p53–MDM2 binding. Thus, our technique provides a unique methodology for the development of novel therapeutic approaches based on intracellular targeting.

Keywords: Tat; HA2; nuclear localization signal; intracellular targeting; peptide aptamer

Progress in molecular biological research on intractable diseases such as cancer is steadily increasing our knowledge of the mechanisms of malignant transformation occurring in tumor cells. However, the complexity of biological interactions makes it increasingly difficult to predict gene and protein functions as we proceed from the immediate metabolic pathway to the levels of the cell and organism. Especially at the cellular level, a variety of tools are available to determine protein function and to develop novel therapeutic approaches, including antisense, peptide modulators, proteins and the overexpression of wild-type or dominant-negative proteins. Small peptides might be able to complement these agents because of

T.S. and T.Y. contributed equally to this work.

*Corresponding author. Laboratory of Pharmaceutical Proteomics, National Institute of Biomedical Innovation, 7-6-8 Saito-Asagi, Ibaraki, Osaka 567-0085, Japan.
E-mail address: tsunoda@nibio.go.jp.

† T.S. and T.Y. contributed equally to this work.

Abbreviations used: MDM2, mouse double minute 2; PTD, protein transduction domain; HA2, hemagglutinin-2 subunit; NLS, nuclear localization signal; NLS–VENUS–Tat, VENUS protein with Tat, NLS and His tag; Tat–cargo, Tat-fused cargo; HA2–Tat, Tat-fused endosome-disruptive HA2 peptide; PM10–Tat, Tat-fused PM10; NLS–PM10–

their ability to recognize specific protein domains and thus to interfere with enzymatic functions or protein–protein interactions.[1] Furthermore, these peptides, designated "peptide aptamers," seem to be non-genotoxic and useful for adjunct chemotherapy. However, these approaches are often limited by an inability to effectively deliver the agents to the appropriate cellular location.

Because a prerequisite for their intracellular action is their delivery into cells, various intracellular delivery approaches, such as protein transduction technology with protein transduction domains (PTDs; e.g., Tat, Antp, VP22, Rev and so on), are currently undergoing intensive scrutiny.[2,3] However, protein transduction technology using PTDs has some disadvantages, one of which is the accumulation of PTDs or PTD-fused peptides in the endocytic compartment. We and others have reported that the main mechanism of protein transduction is penetration into cells by macropinocytosis and that therefore much of the material taken up remains entrapped in the macropinosomes.[4–7] Another disadvantage is that there is no technique for controlling the intracellular distribution of peptide aptamers such that their effects are extremely limited. For these reasons, it is important that peptide aptamers be delivered directly into specific cellular compartments. Because optimal approaches for overcoming these disadvantages have not yet been developed, high concentrations of PTDs or PTD-fused peptides must still be employed in order for the technology to function effectively.

With this in mind, we focused on developing intracellular targeting technology for peptide aptamers fused with Tat protein basic domain residues 47–57 (YGRKKRRQRRR) from human immunodeficiency virus-1 in the context of cancer therapeutics. We recently reported that survivin-targeted peptide aptamers (shepherdin) linked to the NH_2-terminal domain of the influenza virus hemagglutinin-2 subunit (HA2), which is a pH-dependent fusogenic peptide inducing lysis of membranes at low pH levels,[8,9] are efficiently released from macropinosomes. This approach succeeded in inducing the death of survivin-expressing malignant tumor cells.[10] Based on this previous study, here we devised a novel intracellular targeting technology using HA2 and nuclear localization signal (NLS) peptides for converting peptide aptamers into efficient research tools for cell biology and cancer therapeutics. We established for the first time that Tat-conjugated peptide aptamers can be selectively delivered to the nucleus by combining HA2 and NLS peptides. Furthermore, we evaluated the utility of our nuclear targeting method using p53-derived peptide from the human MDM2 (mouse double minute 2, also termed HDM2 in humans)-binding domain (residues 17–26: designated PM10), which is a peptide inhibitor of p53–MDM2 binding.[11] Recent reports suggested that inhibiting p53–MDM2 binding could reactivate the p53 pathway and induce growth-suppressive effects and cell cycle arrest of tumor cells as well as normal cells possessing wild-type p53.[11–17] Because the interaction of p53 and MDM2 takes place inside the nucleus, nuclear delivery of PM10 may potentiate the cytostatic effect of this agent. Indeed, we found that our nuclear targeting technique employing PTD, HA2 and NLS peptides markedly enhanced PM10-mediated cytostatic effects against A549 (human lung adenocarcinoma) and WI-38 (human embryonic fibroblast, lung-derived cell line) cells. These results indicate that our intracellular targeting techniques can deliver the cargo into the appropriate organelle and provide a unique research tool for cellular biology and the development of novel therapeutic approaches.

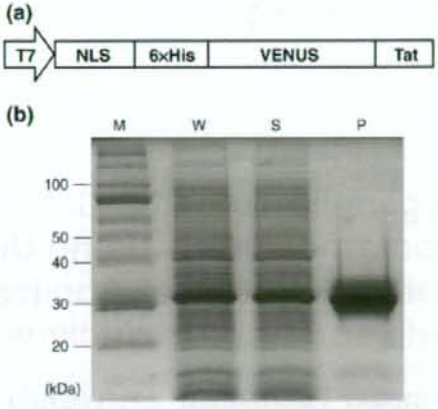

Fig. 1. Vector construction and SDS-PAGE analysis of NLS–VENUS–Tat. (a) Schematic of the NLS–VENUS–Tat region of T7 promoter-driven protein expression vector. The VENUS (variant of yellow fluorescent protein) DNA sequence was kindly provided by Dr. A. Miyawaki (RIKEN Brain Science Institute, Saitama, Japan). The NLS–VENUS–Tat DNA sequence was amplified by PCR. At the 5′ end, the primer sequence 5′-AA CTT TAA GAA GGA GAT ATA *CAT ATG* CCG AAA AAG AAA CGT AAA GTT ACC ATG GCT CAC CAC CAT CAC CAC CAT **GAC TAC AAA GAC GAT GAT GAC AAA** GAA GCT TAC GTG AGC AAG GGC GAG GAG CTG TT-3′ introduced an NdeI site (italics), an NLS (boldface) and a 6× His tag (underline); at the 3′ end, the primer sequence 5′-T TCC TTT CGG GCT TTG TTA GCA GCC *GAA TTC* TTA TTA **ACG GCG ACG CTG GCG ACG TTT TTT ACG ACC GTA** CTC GAG CTT GTA CAG CTC GTC CAT GCC GAG-3′ introduced an EcoRI site (italics) and a Tat sequence (boldface). The PCR product was digested with NdeI as well as EcoRI and inserted into pT7 vector, under the control of the T7 promoter. (b) The plasmid was transformed into *E. coli* BL21 Star (DE3) (Invitrogen, Carlsbad, CA), and cells expressing VENUS proteins were cultured at 25 °C, 250 rpm, for 6 h. The cell paste was then solubilized in a BugBuster Master Mix (Novagen, Darmstadt, Germany) and centrifuged. NLS–VENUS–Tat was recovered in the supernatant and purified by His-tag affinity purification and gel-filtration chromatography. SDS-PAGE analysis was performed under reducing conditions. Lane M, molecular weight standard; lane W, *E. coli* extracts prepared after induction of expression by IPTG; lane S, soluble fractions; lane P, purified proteins.

Tat-fused cargo can be selectively delivered to the nucleus by combining HA2 and NLS peptides

We constructed a VENUS protein (variant of yellow fluorescent protein) fused with Tat, NLS and His tag (NLS–VENUS–Tat) for use as an expression vector (Fig. 1a). NLS–VENUS–Tat was indeed expressed in *Escherichia coli* [BL21 Star (DE3)] after induction with IPTG. The level of expression of the NLS–VENUS–Tat protein was analyzed by SDS-PAGE in total cell lysates (Fig. 1b). Protein expression was specifically induced because we did not find substantially leaky expression of the recombinant protein (data not shown). Recombinant NLS–VENUS–Tat was produced almost entirely in the soluble fraction and had an apparent molecular mass of about 32 kDa under reducing conditions (Fig. 1b, lane S). Purification was carried out by lysis, and separation of the soluble fraction was carried out by centrifugation. This was then loaded onto a Ni^{2+} column for initial purification. The NLS–VENUS–Tat protein eluted from the Ni^{2+} column was more than 90% pure (Fig. 1b, lane P). The purity, apparent molecular mass and cellular internalization activity of the eluted NLS–VENUS–Tat proteins were established by SDS-PAGE and flow cytometry.

Numerous mechanistic studies have shown that Tat peptides rapidly permeate plasma membranes and translocate into the nucleus.[18–22] This mechanism is currently used to deliver proteins and nucleic acids to cell nuclei through covalent linkages of Tat and cargoes.[18] However, nuclear delivery has remained problematic and very limited, because endosome escape and nuclear transport of Tat-fused cargo (Tat–cargo) represent a passive rather than an active process. Indeed, in HeLa cells treated with NLS–VENUS–Tat alone, only punctate cytoplasmic fluorescence, and no fluorescence in the nucleus, was observed (Fig. 2). We had previously confirmed that Tat-fused VENUS co-localized in live cells to vesicles with FM4-64, which is a general endosome marker (data not shown). Furthermore, FAM (carboxyfluorescein) dye-fused Tat peptides also co-localized in FM4-64-positive endosomal vesicles (data not shown). Thus, these results indicated that much of the NLS–VENUS–Tat was entrapped within the endosomal vesicles, resulting in low levels of nuclear accumulation. It is therefore reasonable to propose that Tat–cargo alone cannot reach the targeted cellular compartment, especially the nucleus, and that the therapeutic effects of anticancer peptide aptamers are extremely limited for this reason. Therefore, we devised an active nuclear targeting technique using endosome-disruptive HA2 and SV40-derived NLS peptides.

Recently, we reported that co-treatment with Tat–cargo and the Tat-fused endosome-disruptive HA2 peptide (HA2–Tat) improved the endosome-escape ability and the tumor-killing activity of Tat-fused antisurvivin peptide aptamers.[10] Therefore, we hypothesized that NLS–VENUS–Tat can be delivered into the nucleus if NLS–VENUS–Tat can be engineered to escape from the endosomal vesicles into the cytosol by co-treatment with HA2–Tat. To investigate whether co-treatment with HA2–Tat does effectively improve the nuclear localization of NLS–Tat–cargo, we co-treated HeLa cells with NLS–VENUS–Tat and HA2–Tat and analyzed the intracellular localization of NLS–VENUS–Tat by confocal laser scanning

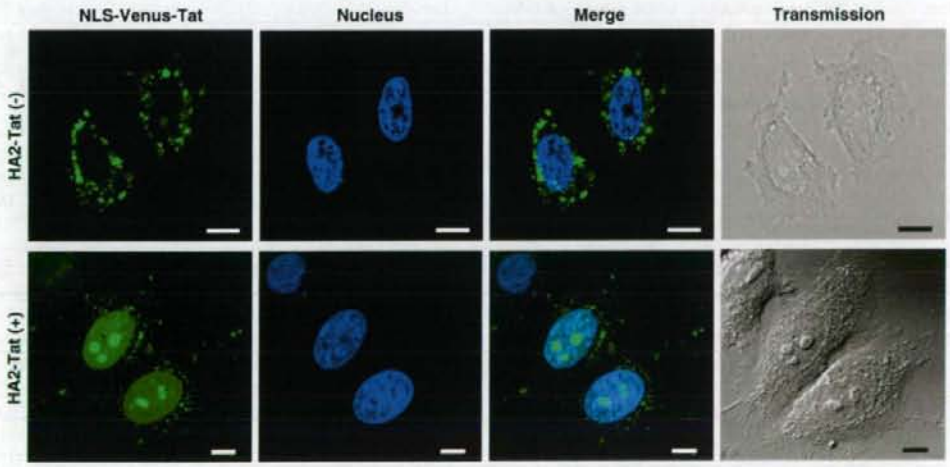

Fig. 2. Intracellular distribution of NLS–VENUS–Tat. HeLa cells were cultured on a Lab-Tek II Chambered Coverglass system (Nalge Nunc International) at 3.0×10^4 cells/well in MEM (minimum essential medium)-α supplemented with 10% fetal bovine serum and incubated for 24 h at 37 °C. Internalization of NLS–VENUS–Tat was performed as follows: HeLa cells were co-treated with NLS–VENUS–Tat (10 μM) with or without HA2–Tat (5 μM) in Opti-MEM I (Invitrogen) containing 100 ng/ml of Hoechst 33342 (Invitrogen). After incubation at 37 °C for 3 h, the medium was changed for a fresh medium and assessed by confocal laser scanning microscopy (Leica Microsystems GmbH, Wetzlar, Germany) without cell fixation. Scale bars in each photomicrograph represent 10 μm.

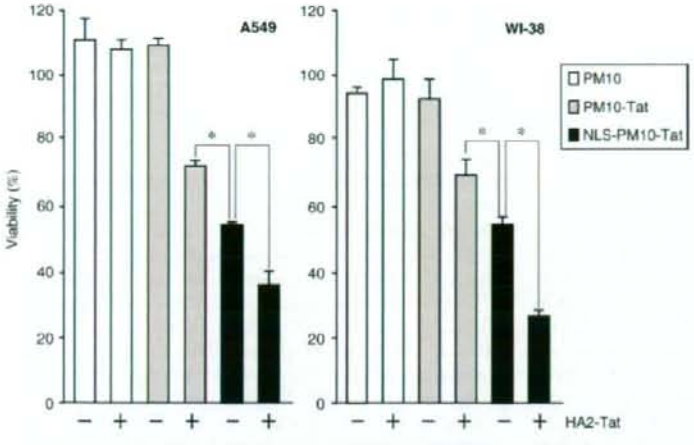

Fig. 3. Nuclear targeting potentiates the cytostatic effect of PM10. All peptides used in this study were purchased from GL Biochem Ltd. (Hiroshima, Japan) with confirmed purities >90% by HPLC and mass spectrography. The sequences of these peptides were GLFEAIEGFIENGWEGMIDGWYG**YGRKKRRQRRR** for HA2–Tat, ETFSDLWKLL for PM10, ETFSDLWKLL**YGRKKRRQRRR** for PM10–Tat and PKKKRKVETFSDLWKLL**YGRKKRRQRRR** for NLS–PM10–Tat. Tat and NLS are shown in boldface and underlined, respectively. A549 or WI-38 cells were seeded into 96-well tissue culture plates (Nalge Nunc International) at 1.0×10^4 cells/well. After incubation for 24 h at 37 °C, the cells were treated with PM10, PM10–Tat or NLS–PM10–Tat at 6 μM (for A549 cells) or 12 μM (for WI-38 cells) in the presence or absence of HA2–Tat (5 μM). After 6 h (for A549 cells) or 24 h (for WI-38 cells), cell viability was determined with the use of WST-8 assay (Nakalai Tesque Inc., Kyoto, Japan) according to the manufacturer's protocol. Data are presented as the mean±SD of triplicate assays. Statistical treatment of the data was performed according to Student's *t* test for two populations (*$p<0.01$).

microscopy (Fig. 2). Co-treatment of HeLa cells with NLS–VENUS–Tat and HA2–Tat resulted in nuclear localization of VENUS, co-localized with Hoechst 33342-stained nuclei. This finding documents that Tat–cargo can be selectively delivered to the nucleus by using HA2 and NLS peptides. Although several groups have attempted to deliver macromolecular drugs to specific organelles, they used PTDs conjugated only with an organelle-targeting signal, such as NLS or mitochondria-targeting signal.[23,24,25] Our data revealed that NLS–VENUS–Tat was entrapped within the endosomal vesicles, with no detectable fluorescence derived from VENUS found in the nucleus. This indicates that organelle targeting by signal-fused PTD–cargo alone does not allow efficient migration into the targeted organelle in the absence of an endosome-escape strategy. Although the influence of the use of different cell types, fluorescent dye, cargo, incubation time and so on could not be excluded as contributing to targeting inability, we found that nuclear transport efficiency could be augmented by combining PTD, HA2 and NLS peptides. Furthermore, our results imply that macromolecules could be delivered into other organelles, such as mitochondria, endoplasmic reticulum and peroxisomes, using different organelle-targeting signal sequences. To this end, we are currently developing novel intracellular drug delivery systems that can target macromolecules into different organelles in a manner analogous to our nuclear targeting techniques.

Nuclear targeting enhances the cytostatic activity of anti-MDM2 peptide aptamer

Next, we tested the utility of our nuclear targeting method using the MDM2-binding peptide aptamer, PM10, which is a p53-derived peptide corresponding to a sequence within the MDM2-binding domain. Kanovsky *et al.* reported that PTD-mediated intracellular delivery of PM10 could reactivate p53 and induce p53-mediated apoptosis of tumor cells with wild-type p53.[11] Under physiological conditions, growth-suppressive and proapoptotic activity of p53 is inhibited by MDM2, which binds p53 and negatively regulates its activity and stability.[16] Recent reports indicated that prevention of p53–MDM2 binding activates the p53 signaling pathway and induces p53-dependent apoptosis in cancer cells possessing wild-type p53.[12,14,15] In addition, the abrogation of p53–MDM2 binding mediates a cytostatic effect and cell cycle arrest in proliferating normal cells.[13,15,17] Because PM10 seems to bind nuclear-localized MDM2 and inhibits MDM2-inducible ubiquitination and degradation of p53, we hypothesized that the nuclear targeting method using HA2 and NLS peptides would enhance its cytotoxicity. To test this, we investigated the effects of treatment with PM10 on cell viability using A549 (human lung adenocarcinoma) and WI-38 (human lung-derived embryonic fibroblast) cells, which possess wild-type p53 (Fig. 3). In A549 and WI-38 cells treated with PM10, Tat-fused PM10 (PM10–Tat) grew vigorously. However, co-treatment with HA2–Tat and PM10–Tat together markedly inhibited A549 and WI-38 cell growth. Furthermore, A549 and WI-38 cells co-treated with HA2–Tat and NLS-fused PM10–Tat (NLS–PM10–Tat) showed greater growth inhibition compared with those treated with NLS–PM10–Tat alone. According to a report from the developers of PM10, although transduction of PTD-fused PM10 (PM10-PTD) into cancer cells could induce tumor cell death *in vitro* and *in vivo*, a high concentration of PM10-PTD was required to see an effect on cancer

cells.[11,26] In contrast, our nuclear targeting technique using PTD, HA2 and NLS peptides markedly enhanced the nuclear localization of the cargo and the PM10-mediated cytostatic effect at low concentrations of PM10. To the best of our knowledge, this is the first report that nuclear targeting of MDM2-binding peptide aptamers can lead to augmentation of cytostatic activity.

In the present study, we aimed to develop a novel cancer therapeutic approach by controlling apoptotic pathways using peptide-based drugs. Recently, the use of intracellular antibodies (intrabodies) directed to a specific target antigen present in the cell has also been suggested as a therapeutic lead to control the apoptotic pathway.[27,28] Our organelle-targeting strategy does seem able to deliver intrabodies directly to the specific organelle in which disease-related proteins reside. Furthermore, we have generated antibodies for various targeted antigens using a non-immune phage scFv library.[29] Thus, we are also currently developing a novel approach to intracellular therapy combining an organelle-targeting strategy and antibody engineering.

Acknowledgements

This study was supported in part by Grants-in-Aid for Scientific Research (20790156) from the Ministry of Education, Culture, Sports, Science and Technology of Japan; in part by a Health and Labor Sciences Research Grant from the Ministry of Health, Labor and Welfare of Japan; in part by a Grant for Industrial Technology Research Program (03A47016a) from the New Energy and Industrial Technology Development Organization of Japan; and in part by funding from the Takeda Science Foundation.

References

1. Mendoza, F. J., Espino, P. S., Cann, K. L., Bristow, N., McCrea, K. & Los, M. (2005). Anti-tumor chemotherapy utilizing peptide-based approaches—apoptotic pathways, kinases, and proteasome as targets. *Arch. Immunol. Ther. Exp.* **53**, 47–60.
2. Dietz, G. P. & Bahr, M. (2004). Delivery of bioactive molecules into the cell: the Trojan horse approach. *Mol. Cell. Neurosci.* **27**, 85–131.
3. Chauhan, A., Tikoo, A., Kapur, A. K. & Singh, M. (2007). The taming of the cell penetrating domain of the HIV Tat: myths and realities. *J. Controlled Release*, **117**, 148–162.
4. Fretz, M., Jin, J., Conibere, R., Penning, N. A., Al-Taei, S., Storm, G. *et al.* (2006). Effects of Na^+/H^+ exchanger inhibitors on subcellular localisation of endocytic organelles and intracellular dynamics of protein transduction domains HIV-TAT peptide and octaarginine. *J. Controlled Release*, **116**, 247–254.
5. Wadia, J. S., Stan, R. V. & Dowdy, S. F. (2004). Transducible TAT-HA fusogenic peptide enhances escape of TAT-fusion proteins after lipid raft macropinocytosis. *Nat. Med.* **10**, 310–315.
6. Sugita, T., Yoshikawa, T., Mukai, Y., Yamanada, N., Imai, S., Nagano, K. *et al.* (2008). Comparative study on transduction and toxicity of protein transduction domains. *Br. J. Pharmacol.* **153**, 1143–1152.
7. Kaplan, I. M., Wadia, J. S. & Dowdy, S. F. (2005). Cationic TAT peptide transduction domain enters cells by macropinocytosis. *J. Controlled Release*, **102**, 247–253.
8. Han, X., Bushweller, J. H., Cafiso, D. S. & Tamm, L. K. (2001). Membrane structure and fusion-triggering conformational change of the fusion domain from influenza hemagglutinin. *Nat. Struct. Biol.* **8**, 715–720.
9. Skehel, J. J., Cross, K., Steinhauer, D. & Wiley, D. C. (2001). Influenza fusion peptides. *Biochem. Soc. Trans.* **29**, 623–626.
10. Sugita, T., Yoshikawa, T., Mukai, Y., Yamanada, N., Imai, S., Nagano, K. *et al.* (2007). Improved cytosolic translocation and tumor-killing activity of Tat-shepherdin conjugates mediated by co-treatment with Tat-fused endosome-disruptive HA2 peptide. *Biochem. Biophys. Res. Commun.* **363**, 1027–1032.
11. Kanovsky, M., Raffo, A., Drew, L., Rosal, R., Do, T., Friedman, F. K. *et al.* (2001). Peptides from the amino terminal mdm-2-binding domain of p53, designed from conformational analysis, are selectively cytotoxic to transformed cells. *Proc. Natl. Acad. Sci. USA*, **98**, 12438–12443.
12. Vassilev, L. T., Vu, B. T., Graves, B., Carvajal, D., Podlaski, F., Filipovic, Z. *et al.* (2004). *In vivo* activation of the p53 pathway by small-molecule antagonists of MDM2. *Science*, **303**, 844–848.
13. Vassilev, L. T. (2004). Small-molecule antagonists of p53–MDM2 binding: research tools and potential therapeutics. *Cell Cycle*, **3**, 419–421.
14. Tovar, C., Rosinski, J., Filipovic, Z., Higgins, B., Kolinsky, K., Hilton, H. *et al.* (2006). Small-molecule MDM2 antagonists reveal aberrant p53 signaling in cancer: implications for therapy. *Proc. Natl. Acad. Sci. USA*, **103**, 1888–1893.
15. Shangary, S., Qin, D., McEachern, D., Liu, M., Miller, R. S., Qiu, S. *et al.* (2008). Temporal activation of p53 by a specific MDM2 inhibitor is selectively toxic to tumors and leads to complete tumor growth inhibition. *Proc. Natl. Acad. Sci. USA*, **105**, 3933–3938.
16. Kubbutat, M. H., Jones, S. N. & Vousden, K. H. (1997). Regulation of p53 stability by Mdm2. *Nature*, **387**, 299–303.
17. Efeyan, A., Ortega-Molina, A., Velasco-Miguel, S., Herranz, D., Vassilev, L. T. & Serrano, M. (2007). Induction of p53-dependent senescence by the MDM2 antagonist nutlin-3a in mouse cells of fibroblast origin. *Cancer Res.* **67**, 7350–7357.
18. Vives, E., Charneau, P., van Rietschoten, J., Rochat, H. & Bahraoui, E. (1994). Effects of the Tat basic domain on human immunodeficiency virus type 1 transactivation, using chemically synthesized Tat protein and Tat peptides. *J. Virol.* **68**, 3343–3353.
19. Vives, E., Brodin, P. & Lebleu, B. (1997). A truncated HIV-1 Tat protein basic domain rapidly translocates through the plasma membrane and accumulates in the cell nucleus. *J. Biol. Chem.* **272**, 16010–16017.
20. Potocky, T. B., Menon, A. K. & Gellman, S. H. (2003). Cytoplasmic and nuclear delivery of a TAT-derived peptide and a beta-peptide after endocytic uptake into HeLa cells. *J. Biol. Chem.* **278**, 50188–50194.
21. Caron, N. J., Quenneville, S. P. & Tremblay, J. P. (2004). Endosome disruption enhances the functional nuclear delivery of Tat-fusion proteins. *Biochem. Biophys. Res. Commun.* **319**, 12–20.

22. Lundberg, M., Wikstrom, S. & Johansson, M. (2003). Cell surface adherence and endocytosis of protein transduction domains. *Mol. Ther.* **8**, 143–150.
23. Shokolenko, I. N., Alexeyev, M. F., LeDoux, S. P. & Wilson, G. L. (2005). TAT-mediated protein transduction and targeted delivery of fusion proteins into mitochondria of breast cancer cells. *DNA Repair (Amst.)*, **4**, 511–518.
24. Del Gaizo, V. & Payne, R. M. (2003). A novel TAT-mitochondrial signal sequence fusion protein is processed, stays in mitochondria, and crosses the placenta. *Mol. Ther.* **7**, 720–730.
25. Matsushita, M., Tomizawa, K., Moriwaki, A., Li, S. T., Terada, H. & Matsui, H. (2001). A high-efficiency protein transduction system demonstrating the role of PKA in long-lasting long-term potentiation. *J. Neurosci.* **21**, 6000–6007.
26. Michl, J., Scharf, B., Schmidt, A., Huynh, C., Hannan, R., von Gizycki, H. *et al.* (2006). PNC-28, a p53-derived peptide that is cytotoxic to cancer cells, blocks pancreatic cancer cell growth *in vivo*. *Int. J. Cancer*, **119**, 1577–1585.
27. Wheeler, Y. Y., Kute, T. E., Willingham, M. C., Chen, S. Y. & Sane, D. C. (2003). Intrabody-based strategies for inhibition of vascular endothelial growth factor receptor-2: effects on apoptosis, cell growth, and angiogenesis. *FASEB J.* **17**, 1733–1735.
28. Williams, B. R. & Zhu, Z. (2006). Intrabody-based approaches to cancer therapy: status and prospects. *Curr. Med. Chem.* **13**, 1473–1480.
29. Imai, S., Mukai, Y., Nagano, K., Shibata, H., Sugita, T., Abe, Y. *et al.* (2006). Quality enhancement of the non-immune phage scFv library to isolate effective antibodies. *Biol. Pharm. Bull.* **29**, 1325–1330.

Laboratory of Pharmaceutical Proteomics[1], National Institute of Biomedical Innovation (NIBIO), Graduate School of Pharmaceutical Sciences[2], Center of Advanced Medical Engineering and Informatics[3], Osaka University, Osaka, Japan

Effect of protein properties on display efficiency using the M13 phage display system

S. Imai[1,2], Y. Mukai[1,2], T. Takeda[1], Y. Abe[1], K. Nagano[1,2], H. Kamada[1,3], S. Nakagawa[2], S. Tsunoda[1,3], Y. Tsutsumi[1,2,3]

Received May 15, 2008, accepted May 21, 2008

Shin-ichi Tsunoda, Ph.D., Laboratory of Pharmaceutical Proteomics, National Institute of Biomedical Innovation (NIBIO), 7-6-8 Saito-Asagi, Ibaraki, Osaka 567-0085, Japan tsunoda@nibio.go.jp

Pharmazie 63: 760–764 (2008) *doi: 10.1691/ph.2008.8132*

The M13 phage display system is a powerful technology for engineering proteins such as functional mutant proteins and peptides. In this system, it is necessary that the protein is displayed on the phage surface. Therefore, its application is often limited when a protein is poorly displayed. In this study, we attempted to understand the relationship between a protein's properties and its display efficiency using the well-known pIII and pVIII type phage display system. The display of positively charged SV40 NLS and HIV-1 Tat peptides on pIII was less efficient than that of the neutrally charged RGDS peptide. When different molecular weight proteins (1.5–58 kDa) were displayed on pIII and pVIII, their display efficiencies were directly influenced by their molecular weights. These results indicate the usefulness in predicting a desired protein's compatibility with protein and peptide engineering using the phage display system.

1. Introduction

Phage display systems have attracted much attention as the best technology to create functional mutant proteins and peptides ever since Smith et al. reported that random peptides could be displayed on the surface of filamentous M13 phage (Smith 1985). Many researchers have applied this system in attempts to create human antibodies and tissue-specific peptides (Schier et al. 1996; Maruta et al. 2003; Imai et al. 2006). Indeed, we have been successful in creating a useful mutant TNF to be used as a drug (Shibata et al. 2004; Yamamoto et al. 2003). Thus, the phage display system has a wide range of applications (Stich et al. 2003; Gourdine et al. 2005; Takashima et al. 2000).

Filamentous M13 phage has a circular single stranded DNA and takes the form of a long tube that consists of eleven kinds of proteins. This virus effectively proliferates upon infection of *E. coli* (Sidhu 2001; Bayer and Feigenson 1985; Kuhn 1987). In the phage display system, a fusion protein composed of target-molecule and coat protein is derived from a phagemid vector, and wild-type phage composition proteins (pI–pXI) are derived from a helper phage genome. These components can make phage libraries that display target-molecules by assembling within the periplasm of *E. coli*. The most useful characteristic of this system is that protein libraries can be displayed easily on the phage surface by inserting gene libraries within the phage genome. Target-molecules are obtained rapidly by the use of an *in vitro* affinity panning procedure that selects and amplifies specific phage clones (Smith 1985).

In the phage display system, target-molecules can be displayed on coat proteins (pIII, pVI, pVII, pVIII, pIX), though generally they are displayed on pIII or pVIII. Displaying 0–1 molecule per phage in the pIII type phage display system is suitable for isolating high-affinity molecules (Chasteen et al. 2006; Keresztessy et al. 2006). Alternatively, ten molecules can be displayed on a phage particle in the pVIII type phage display system to select low-affinity molecules (Verhaert et al. 1999; Kneissel et al. 1999; Lowman 1997).

As described, the phage display system is the most useful tool to create bioactive peptides and functional mutant proteins. However, because the efficiency of display is influenced by the properties of the target protein (molecular weight, electric charge, etc.), poor display often limits its application. Despite this problem, there is little research examining the relationship between display efficiency and a protein's properties. Thus, studies are warranted in order to apply the phage display system effectively. In this report, we prepared phages that displayed proteins of different molecular weights and electric charges to ascertain the relationship between display efficiency and protein properties.

2. Investigations, results and discussion

In this study we examined the relationship between protein properties (molecular weight, electric charge etc.) and the efficiency of display with pIII and pVIII coat proteins of the filamentous M13 phage display system (Fig. 1). To begin with, we prepared phages that displayed different electrically charged peptides on pIII (Fig. 2B) and evalu-

A)

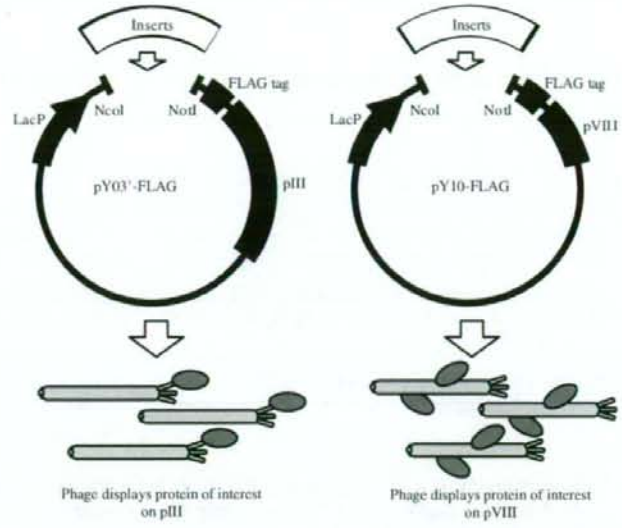

B)

Inserts	Molecular weight (Da)	pI
RGDS peptide (RGDS)	443	6.4
SV40 NLS peptide (PKKKRKV)	883	11.9
HIV-Tat peptide (YGRKKRRQRRR)	1,559	12.8
LacZ-α	11,000	5.2
anti-KDR scFv	25,000	5.0
Importin-α	58,000	5.1

Fig. 1:
Construction of phagemid vectors encoding different proteins or peptides.
A) Different inserts were cloned into pY03'-FLAG and pY10-FLAG phagemid vectors. Phage particles displaying proteins fused to pIII and pVIII were prepared from pY03'-FLAG and pY10-FLAG, respectively. B) Different inserts and their molecular weights

A)

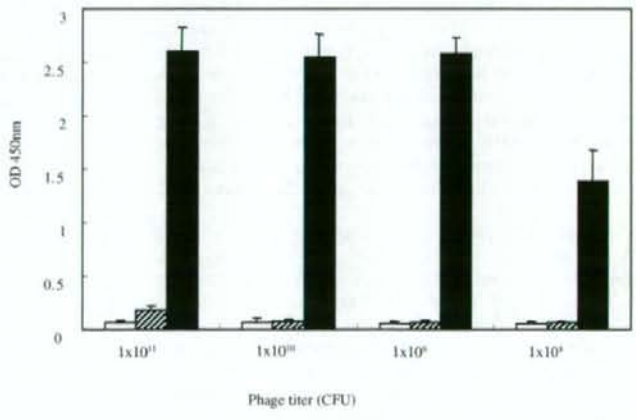

B)

	sequence	M.W. (Da)	pI
□ Tat peptide	YGRKKRRQRRR	1,559	12.8
▩ SV40 NLS	PKKKRKV	883	11.9
■ RGDS peptide	RGDS	433	6.4

Fig. 2:
Influence of the efficiency of peptide-display by the ionic charge of peptides.
The efficiency of peptide-display on pIII was assessed by phage ELISA. Displayed peptides were fused to FLAG-tag – pIII on the phage particle and captured by immobilized anti-FLAG antibody. After washing, the number of captured phage was assessed by anti-M13 HRP conjugate. Two positively charged peptides (Tat peptide; □ and SV40 NLS; ▩) and a neutral peptide (RGDS; ■) were used in this experiment (n = 3). Each data value represents the mean ± S.D. B) Sequences of displayed peptides and their pIs. Cationic amino acids are underlined. All pI values were calculated by Expasy Compute pI/Mw tool (http://au.expasy.org)

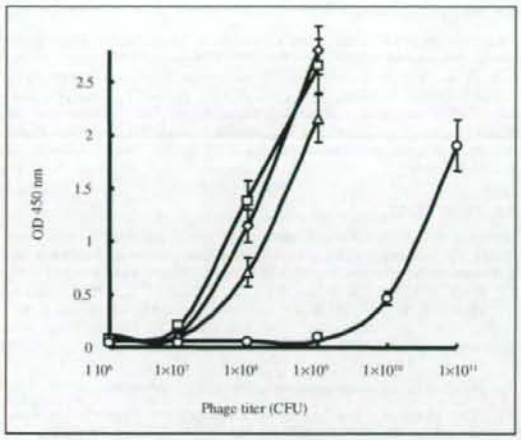

Fig. 3: Comparison of the efficiency of protein-display using pIII type phage display.
The efficiency of protein-display on pIII was assessed by phage ELISA. Proteins with different molecular weights (approximately 400–58,000 Da) were displayed on phage particle as pIII fusion proteins. This experiment was performed using the same method as Fig. 2 (n = 3). Each data value represents the mean ± S.D. □, RGDS-pIII phage; ◇, LacZ-pIII phage; △, scFv-pIII phage; ○, Importin-α-pIII phage

ated the relationship between electric charge and display efficiency using FLAG tagged ELISA (Fig. 2A). The display of positively charged SV40 NLS and HIV-1 Tat peptides were less efficient than that of the neutrally charged RGDS peptide. Generally, positively charged peptides are easy to adsorb onto various surfaces (Gaillard et al. 1999), and they repulse each other. Therefore, positively charged peptides may interfere with phage assembly in the periplasm.

Second, we examined the relationship between molecular weight and display efficiency again using FLAG tagged ELISA (Fig. 3). Because the display of positively charged sample was less efficient (Fig. 2), we used the neutrally charged proteins (pI 5.0–6.4) (MW 1.5–58 kDa) displayed on pIII to examine the influence of molecular weight on display. Phage displaying the low molecular weight RGDS peptide bound to anti-FLAG antibody at a concentration of 10^6–10^9 CFU. The higher molecular weight importin-α (58 kDa) displayed on the phage surface could not bind at the same concentration, needing 10^9–10^{11} CFU. In general, the amount of phage prepared by following the standard protocol was approximately 10^{12}–10^{13} CFU (Imai 2006). To create functional mutants using a phage library, it is desirable to use an amount of phage in excess (more than 100-fold) of the phage library (approximately 10^6–10^9 CFU). When proteins display on the phage surface efficiently, the experiment can proceed without bias. However, our result suggests that a phage library displaying high molecular weight proteins may be of low quality simply because the levels of the desired proteins are not sufficiently expressed for screening. This introduces a selection bias for those proteins that can be expressed at the proper level.

To examine the efficiency of pIII-display in greater detail, we quantified the number of molecules displayed on the phage surface by electrophoresis analysis using CsCl purified phage (Fig. 4). These results (Fig. 3, 4) demonstrate that the efficiency of RGDS peptide-display on pIII was the best (approximately 2 molecules/phage). The display efficiency decreased as the molecular weight of the target protein increased. Because the titer of all phages prepared in this experiment was determined, we suggested that the display of different molecular weight proteins did not affect the efficiency of phage-preparation (data not shown). Additionally, the proteins used in this experiment (RGDS, LacZ, scFv and importin-α) were expressed efficiently in *E. coli*. Therefore, we suggest that the efficiency with which a protein is displayed on pIII is directly related to its molecular weight.

Finally, we examined the efficiency of pVIII-display by Western blot and confirmed that it also decreased as the molecular weight increased (Fig. 5). Interestingly, this result shows that scFv (25 kDa) could be displayed on pVIII efficiently. Because the pVIII phage display system is generally believed to be limited in its application precisely by the molecular weight of displayed protein, many used it only for display of peptide libraries (Verhaert et al. 1999; Kneissel et al. 1999; Lowman 1997; Gaillard et al. 1999). However, our result suggests that the pVIII system could be applied to larger molecules. This could provide useful

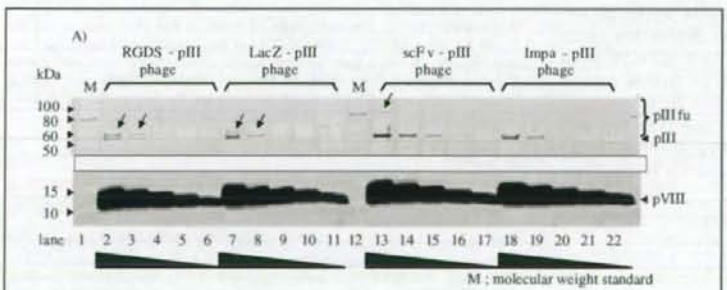

B)

	RGDS-pIII	LacZ-pIII	scFv-pIII	Impα-pIII
M.W. of displayed protein (kDa)	1.5	11	25	58
M.W. of pIII fusion protein (kDa)	52.5	62	76	109
Number of displayed proteins/phage	2.7	1.0	0.12	N.D.

N.D.; Not Detectable

Fig. 4:
Calculated quantity of pIII displayed proteins using Sypro® Ruby staining.
A) The efficiency of display on pIII was quantified using CsCl purifed phages. RGDS-pIII (lanes 2–6), LacZ-pIII (lanes 7–11), scFv-pIII (lanes 13–17) and Impα-pIII phage (lanes 18–22) were used in this experiment. Molecular weight standard was loaded in lanes 1 and 12. Starting from the left, 1×10^{13} vp, 3.3×10^{12} vp, 1.1×10^{12} vp, 3.7×10^{11} vp and 1.2×10^{11} vp were loaded. B) The number of displayed proteins per one phage particle was calculated by fluorescence image analysis. Fluorescence intensity was quantified by Typhoon image analyzer

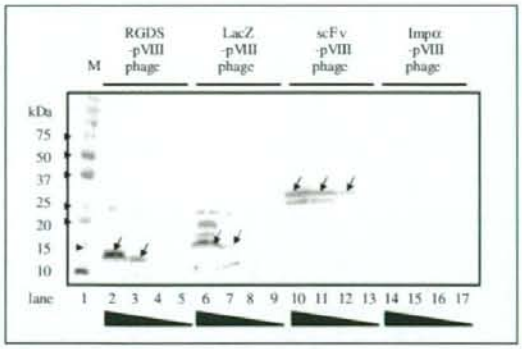

Fig. 5: Comparison of the efficiency of pVIII display protein on phage particles.
The efficiency of display on pVIII was assessed by anti-FLAG western blot. PEG-purified RGDS-pVIII (lanes 2–5), LacZ-pVIII (lanes 6–9), scFv-pVIII (lanes 10–13) and Impα-pVIII phage (lanes 14–17) were used in this experiment. Molecular weight standard was loaded in lane 1. Starting from the left, 1.5×10^{11} cfu, 5×10^{10} cfu, 1.7×10^{10} cfu and 5.5×10^{9} cfu were loaded

additional information by expanding the application of phage display systems to create various mutant proteins.
In this study, different kinds of sample peptides (SV40 NLS, HIV-1 Tat, RGDS) and proteins (RGDS, LacZ, scFv, importin-α) that could be readily expressed in *E. coli* were used as model molecules. The display of positively charged SV40 NLS and HIV-1 Tat peptides on pIII was less efficient than that of the neutrally charged RGDS peptide. When different molecular weight proteins (1.5–58 kDa) were displayed on pIII and pVIII, their display efficiencies were directly related to their molecular weights.
When comparing the efficiency of display between the four model proteins, additional factors (i.e. refolding efficiency, etc.) may account for the differences. These results show at least that the electric charge affected the efficiency of phage display and that high molecular weight proteins could not be displayed on the phage surface successfully. Recently, it was reported that improving the phagemid vector provided better efficiency of protein refolding in *E. coli* and enhanced protein display on the phage surface (Guo et al. 2003). Consequently many hope that the display efficiency of various molecules could be improved using this methodology. However, while this method improves the quality of fusion protein expression, it does not take into account the efficiency of protein assembly for the construction of phage particles. Therefore, it is still important to be able to predict the molecules that will be compatible for protein and peptide engineering using phage display by understanding the properties of this system as they were described in this report.

3. Experimental

3.1. Phagemid vectors and inserts

The pY03′-FLAG phagemid vector was modified from pCANTAB-5E (GE Healthcare Ltd.). To create this vector, the E-tag from the original vector was changed to a FLAG tag (DYKDDDDK). The pY10-FLAG phagemid vector was constructed by replacing the pIII gene in pY03′-FLAG with the pVIII gene. Genes encoding peptides (RGDS, HIV-Tat, SV40 NLS) were synthesized by Operon Biotechnologies Inc., USA. The lacZ-α gene had already been cloned into pY03′-FLAG and pY10-FLAG. The anti-KDR scFv gene was isolated from an optimized non-immune phage antibody library previously described (Imai et al. 2006). The human importin-α gene was amplified from a human bone marrow cDNA library (TAKARA Bio. Inc.). These inserts were digested and cloned into each phagemid vector.

3.2. Phage preparation

Phage was prepared by following a standard protocol. Briefly, phage particles were prepared from *Escherichia coli* (TG1 strain, Stratagene corporation) by co-infection with M13KO7 helper phage (Invitrogen Corporation). Amplified phage in culture media was roughly purified by PEG precipitation. Part of the purified phage was added to the TG1 bacteria, and the phage titer (cfu) was calculated by counting infected TG1 colonies. If necessary, additional purification using a CsCl gradient was performed as described below.

3.3. Phage ELISA

Immunoplates (Nalge Nunc International) were immobilized with anti-FLAG M2 antibody (Sigma-Aldrich Corporation) diluted to 5 μg/ml in bicarbonate buffer (Sigma-Aldrich Corporation). Plates were blocked with 2% block ace (Nakarai Tesque Inc.) for 2 h at 37 °C. Phage solution (PEG-purified) in 0.4% block ace was serially diluted and applied to the wells. After a 1 h incubation at room temperature, the binding phage was detected by anti-M13 HRP conjugate (GE Healthcare Ltd.).

3.4. Purification of phage particles under CsCl gradient

Amplified phage was purified by PEG precipitation. Phage pellets were resuspended in TBS buffer. CsCl powder (IWAI chemicals company) and additional TBS buffer were added to the phage solution up to 31%. After CsCl gradient ultracentrifugation at 400,000 × g at 5 °C for 20 h, the concentrated phage band was isolated. TBS (five volumes) was added to the purified phage and centrifuged again at 400,000 × g at 5 °C for 4 h to remove the CsCl. The obtained phage was resuspended in TBS and used for experiments.

3.5. Sypro Ruby staining

After purifying the phage under a CsCl gradient, the number of phage particles (vp/ml) was estimated from its absorbance according to the standard protocol. Serially diluted phage samples were resolved by SDS – poly acrylamide electrophoresis (SDS-PAGE). Gels were incubated in SYPRO® Ruby protein gel stain reagent (Pearce Biotechnology, Inc., USA) overnight at room temperature. After washing with wash buffer (10% methanol and 7% acetic acid) for 30 min, fluorescence was detected using the Typhoon Variable Image Analyzer (GE Healthcare Ltd.). The number of surface-displayed proteins was calculated from fluorescence intensity using ImageQuant TL software (GE Healthcare Ltd.) assuming that one phage particle contained five pIII coat proteins on its surface.

3.6. Anti-FLAG western blotting

SDS-PAGE was performed using serially diluted phage purified by PEG precipitation. Phage protein in the gel was transferred to PVDF membrane (GE Healthcare Ltd.) using the Hoefer TE 70 semi dry transfer unit (GE Healthcare Ltd.). Membranes were blocked in 4% block ace for 1 h. FLAG-tagged pVIII fusion protein was detected with anti-FLAG M2 antibody (Sigma-Aldrich Corporation) and anti-mouse IgG HRP conjugate (Sigma-Aldrich Corporation). After detection by ECL plus reagent (GE Healthcare Ltd.), its luminescence was quantitated using the LAS-3000 Lumi Imager (Fujifilm Corporation).

Acknowledgements: This study was supported in part by Grants-in-Aid for Scientific Research (No. 20015052) from the Ministry of Education, Culture, Sports, Science and Technology of Japan, by Health and Labor Sciences Research Grant from the Ministry of Health, Labor and Welfare of Japan, and in part by Research Fellowships for Young Scientists (No. 3608) from Japan Society for the Promotion of Science.

References

Bayer R, Feigenson GW (1985) Reconstitution of M13 bacteriophage coat protein. A new strategy to analyze configuration of the protein in the membrane. Biochim Biophys Acta 815: 369–379.
Chasteen L, Ayriss J, Pavlik P, Bradbury AR (2006) Eliminating helper phage from phage display. Nucleic Acids Res 34: e145.
Gaillard C, Flavin M, Woisard A, Strauss F (1999) Association of double-stranded DNA fragments into multistranded DNA structures. Biopolymers 50: 679–689.
Gourdine JP, Greenwell P, Smith-Ravin E (2005) Application of recombinant phage display antibody system in study of Codakia orbicularis gill proteins. Appl Biochem Biotechnol 125: 41–52.
Guo JQ, You SY, Li L, Zhang YZ, Huang JN, Zhang CY (2003) Construction and high-level expression of a single-chain Fv antibody fragment specific for acidic isoferritin in Escherichia coli. J Biotechnol 102: 177–189.
Imai S, Mukai Y, Nagano K, Shibata H, Sugita T, Abe Y, Nomura T, Tsutsumi Y, Kamada H, Nakagawa S, Tsunoda S (2006) Quality enhancement of the non-immune phage scFv library to isolate effective antibodies. Biol Pharm Bull 29: 1325–1330.

Keresztessy Z, Csosz E, Harsfalvi J, Csomos K, Gray J, Lightowlers RN, Lakey JH, Balajthy Z, Fesus L (2006) Phage display selection of efficient glutamine-donor substrate peptides for transglutaminase 2. Protein Sci 15: 2466–2480.

Kneissel S, Queitsch I, Petersen G, Behrsing O, Micheel B, Dubel S (1999) Epitope structures recognised by antibodies against the major coat protein (g8p) of filamentous bacteriophage fd (Inoviridae). J Mol Biol 288: 21–28.

Kuhn A (1987) Bacteriophage M13 procoat protein inserts into the plasma membrane as a loop structure. Science 238: 1413–1415.

Lowman HB (1997) Bacteriophage display and discovery of peptide leads for drug development. Annu Rev Biophys Biomol Struct 26: 401–424.

Maruta F, Parker AL, Fisher KD, Murray PG, Kerr DJ, Seymour LW (2003) Use of a phage display library to identify oligopeptides binding to the lumenal surface of polarized endothelium by ex vivo perfusion of human umbilical veins. J Drug Target 11: 53–59.

Schier R, Bye J, Apell G., McCall A, Adams GP, Malmqvist M, Weiner LM, Marks JD (1996) Isolation of high-affinity monomeric human anti-c-erbB-2 single chain Fv using affinity-driven selection. J Mol Biol 255: 28–43.

Shibata H, Yoshioka Y, Ikemizu S, Kobayashi K., Yamamoto Y, Mukai Y, Okamoto T, Taniai M, Kawamura M, Abe Y, Nakagawa S, Hayakawa T, Nagata S, Yamagata Y, Mayumi T, Kamada H, Tsutsumi Y (2004) Functionalization of tumor necrosis factor-alpha using phage display technique and PEGylation improves its antitumor therapeutic window. Clin Cancer Res 10: 8293–8300.

Sidhu SS (2001) Engineering M13 for phage display. Biomol Eng 18: 57–63.

Smith GP (1985) Filamentous fusion phage: novel expression vectors that display cloned antigens on the virion surface. Science 228: 1315–1317.

Stich N, Van Steen G, Schalkhammer T (2003) Design and peptide-based validation of phage display antibodies for proteomic biochips. Comb Chem High Throughput Screen 6: 67–78.

Takashima A, Mummert M, Kitajima T, Matsue H (2000) New technologies to prevent and treat contact hypersensitivity responses. Ann N Y Acad Sci 919: 205–213.

Verhaert RM, Van Duin J, Quax WJ (1999) Processing and functional display of the 86 kDa heterodimeric penicillin G acylase on the surface of phage fd. Biochem J 342: 415–422.

Yamamoto Y, Tsutsumi Y, Yoshioka Y, Nishibata T, Kobayashi K., Okamoto T, Mukai Y, Shimizu T, Nakagawa S, Nagata S, Mayumi T (2003) Site-specific PEGylation of a lysine-deficient TNF-alpha with full bioactivity. Nat Biotechnol 21: 546–552.